Reverse bifurcations in a unimodal queueing model

James A. Walsh

Department of Mathematics, Oberlin College, Oberlin, OH 44074-1019, USA

Abstract

We present a family of unimodal maps, arising from a simple queueing model, which exhibits reverse bifurcations. We compare and contrast this with bifurcations occurring in the well-known logistic family of unimodal quadratic maps.

Keywords: Period-doubling, tangent, and reverse bifurcation; Unimodal map; Queueing system

1. Introduction

In a recent paper in this journal [1], Frame and Meachem presented computer experiments in which a quartic family of one-dimensional maps exhibited reverse bifurcations. In particular, tangent and period-doubling bifurcations, well-known to occur in the logistic family [2], appear in this quartic family with both forward and reverse orientations. In this paper we present a unimodal (or one-hump) one-dimensional map, derived from a simple queueing model, which exhibits bifurcations akin to those found in the study of the quartic family. Interestingly, reverse bifurcations occur in mappings much less topologically sophisticated than a three-hump quartic function.

2. Bifurcations

The road to chaos for one-dimensional maps often follows a sequence of period-doubling bifurcations as a parameter increases, as illustrated by the logistic family $L_k(x) = kx(1-x)$. It is easy to check that if $k \in [0,4]$, then for any $x_0 \in [0,1]$, $L_k(x_0) \in [0,1]$. For such k, the *orbit* of x_0, defined to be the set $\mathcal{O}^+(x_0) = \{x_0, x_1 = L_k(x_0), x_2 = L_k(x_1), ...\}$, remains bounded within $[0,1]$. Of interest is how orbits $\mathcal{O}^+(x_0)$ change as the parameter k increases.

The simplest way to proceed is via computer simulation. In Fig. 1 we plot the long-term behavior of $\mathcal{O}^+(0.5)$ versus k. That is, for a given k, we compute the first 200 terms in $\mathcal{O}^+(0.5)$, then plot iterates 101-200 vertically above k. The resulting plot is called

an *orbit diagram*. The choice of $x_0 = 0.5$ is due to a result of Singer [3], which states that for a map having negative Schwarzian derivative, any attracting periodic behavior must draw in the orbit of a critical point. One can show L_k has negative Schwarzian derivative, with $x_0 = 0.5$ its sole critical point.

As this remarkable diagram is discussed at length in [1], we focus here on the two types of bifurcations which occur within. Note that for k slightly less than 3, $\mathcal{O}^+(0.5)$ converges to a stable fixed point (depending on k). A *fixed point* is a point of intersection of the graph of L_k and the line $y = x$; it is *stable* if it attracts orbits which start nearby. As proven in [2], a fixed point $x = p$ is stable if $|L_k'(p)| < 1$. A *period n-point* $x = q$ is a fixed point of the n-fold composition $L_k^n(x)$, and it is stable if $|(L_k^n)'(q)| < 1$. The orbit of a period n-point is called an *n-cycle*. An orbit which starts sufficiently close to any point in a stable n-cycle will limit on that period-n behavior over time.

For k slightly larger than 3, $\mathcal{O}^+(0.5)$ converges to a stable 2-cycle. This *period-doubling bifurcation* as k increases through 3 is illustrated in Fig. 2. Note that the fixed point $x = p_k$ changes from stable to *unstable* (that is, $|L_k'(p_k)| > 1$ so that orbits which start nearby move away). As k continues to increase, a stable 4-cycle appears via a period-doubling bifurcation of the function $L_k^2(x)$, followed by a stable 8-cycle arising in a period-doubling bifurcation of the function $L_k^4(x)$, and so on. These period-doublings continue until $k \approx 3.57$, where chaos first appears.

The second type of bifurcation occurring in the logistic family is a *tangent bifurcation*. Note the 3-cycle appearing out of the chaotic morass in Fig. 1. The function $L_k^3(x)$ undergoes a tangent bifurcation at $k \approx 3.828$, as illustrated in Fig. 3. Thus, L_k progresses from having no 3-cycles, to one 3-cycle, and then to a stable-unstable pair of 3-cycles as k increases through 3.828.

It is quite fun investigating the plot in Fig. 1 by zooming in on various regions—it is indeed a surprisingly rich diagram. Regardless of how you search, however, you will find only period-doubling and tangent bifurcations. In addition, once a cycle is created, it persists, though it changes from stable to unstable as discussed above. That this is the case follows from work of Milnor and Thurston [4]. That this need not be the case for quartic maps is the substance of [1]. In the following we present a unimodal map with period-doubling, tangent and reverse bifurcations similar to those found in the quartic family. Here, unimodal means that the map has one critical point c, and is either increasing for $x < c$ and decreasing for $x > c$, or vice versa. Note that while all quadratic maps are unimodal, a unimodal map need not be quadratic.

Interestingly, our unimodal map arises in a simple queueing model [5].

3. A queueing model

Suppose a component of a queueing system consists of a server with a queue of size two (see Fig. 4). Each time period two jobs A and B arrive in the queue at constant rates α and β, respectively. The server will devote ϕ_A and ϕ_B time units to jobs A and B each time period. Letting x_n and y_n denote the lengths of queues A and B at the n^{th} time period, assume ϕ_A and ϕ_B are each functions of the difference $x_n - y_n$ in queue lengths. We also assume the server devotes more time to the job having the longer queue, and further that this component of the network is closed in the sense that the server's capacity equals the sum of the input rates. After normalizing, we have

$$\alpha + \beta = \phi_A + \phi_B = 1. \tag{1}$$

Note that $\alpha, \beta \in (0, 1)$.

The evolution equations for the queue lengths are then given by

$$x_{n+1} = x_n + \alpha - \phi_A(x_n - y_n) \tag{2}$$

$$y_{n+1} = y_n + \beta - \phi_B(x_n - y_n). \tag{3}$$

In adding (2) and (3) and using (1), we see that $x_{n+1} + y_{n+1} = x_n + y_n$, so that for all n, $x_n + y_n = C$, C a constant. Plugging $y_n = C - x_n$ into (2) and setting $C = 2$ to ensure sufficient workload [5], we have

$$x_{n+1} = x_n + \alpha - \phi_A(2x_n - 2). \tag{4}$$

We need only specify ϕ_A to complete the model. The simplest choice would be an all-or-nothing function, in which case the server devotes the entire time period to the job having the longer queue (see Fig. 5). However, this choice reduces (4) to a family of rigid rotation circle maps [5], the dynamics of which are well-understood [6].

A second possibility is the S-shaped curve sketched in Fig. 5. Such a curve is increasing, has a unique inflection point $\hat{x}$, and is concave up for $x < \hat{x}$ and concave down for $x > \hat{x}$. (In Fig. 5, $\hat{x} = 0$.) If we include a parameter which adjusts the steepness of the graph at $\hat{x}$, then this function can be viewed as an approximation to the all-or-nothing case. In all that follows, we choose such an S-shaped curve by setting $\phi_A(x) = 1/(1 + e^{-\lambda x})$, $\lambda > 0$, in which case (4) becomes

$$x_{n+1} = f_{\alpha,\lambda}(x_n) = x_n + \alpha - \frac{1}{1 + e^{-2\lambda(x_n - 1)}},\ \alpha \in (0, 1).$$

The orbit of x_0 under $f_{\alpha,\lambda}$ then corresponds to the length of queue A after successive time periods.

4. Dynamics

For $\lambda > 2$, the maps $f_{\alpha,\lambda}$ are *bimodal* (or two-hump) maps as seen in Fig. 6. Moreover, for $\alpha \in (\frac{1}{1+e^4}, \frac{1}{1+e^{-4}}) \approx (0.018, 0.982)$, $\quad f_{\alpha,\lambda} : [0,2] \to [0,2]$, as is easily checked. Assuming these parameter range values, we reduce to a unimodal map as follows.

Let $c^- = c^-(\lambda)$ and $c^+ = c^+(\lambda)$, respectively, denote the left and right critical points of $f_{\alpha,\lambda}$. Note that each depends only on λ. Suppose that for some λ_0, $f_{\alpha,\lambda_0}(c^-) < c^+$. Then f_{α,λ_0} maps the interval $[0, c^+]$ to itself and, moreover, f_{α,λ_0} restricted to $[0, c^+]$ is a unimodal map. In addition, the inequality $f_{\alpha,\lambda_0}(c^-) < c^+$ will hold for an interval of α-values as changing α simply shifts the graph up or down, without changing the critical points. For this λ_0, we then have a one-parameter (namely α) family of unimodal maps $f_{\alpha,\lambda_0} : [0, c^+] \to [0, c^+]$. This is the type of unimodal family which will serve as our example exhibiting reverse bifurcations.

In a similar fashion, if $f_{\alpha,\lambda_1}(c^+) > c^-$ for some λ_1, then $f_{\alpha,\lambda_1} : [c^-, 2] \to [c^-, 2]$ is a unimodal family. In Fig. 7 we plot the (α, λ)-parameter range for which the restriction of $f_{\alpha,\lambda}$ to either $[0, c^+]$ or $[c^-, 2]$ yields a unimodal family as described above. The blue curve corresponds to (α, λ) for which $f_{\alpha,\lambda}(c^-) = c^+$, while the red curve represents (α, λ) with $f_{\alpha,\lambda}(c^+) = c^-$.

In Fig. 8 we plot $f_{\alpha,\lambda}$-orbit diagrams for four different λ-values. We have chosen (α, λ) so that in each case $f_{\alpha,\lambda}$ is a unimodal map which takes the interval $[0, c^+]$ to itself, that is, we restrict $f_{\alpha,\lambda}$ to $[0, c^+]$. As with the logistic map, one can show $f_{\alpha,\lambda}$ has negative Schwarzian derivative, so that if there is attracting periodic behavior the orbit of the critical point c^- will be drawn to it. To generate these diagrams, we thus plot the long-term behavior of $\mathcal{O}^+(c^-)$ as a function of α.

Period-doubling and period-halving bifurcations are clearly evident in Fig. 8(a). Also observe that, although each plot begins with a sequence of period-doubling bifurcations, the complexity of $\mathcal{O}^+(c^-)$ increases with increasing λ. In Fig.8(d), notice the right-most period-5 window. Two close-ups of this window are presented in Fig. 9, in which we see the logistic bifurcation diagram with orientation reversed. Hence, for $\lambda = 8$, $\quad f_{\alpha,8}$ undergoes infinitely many period-halving and reverse tangent bifurcations.

As discussed in [1], this phenomena can be explained via *trapping regions*. In Fig. 10 we focus on a neighborhood of the critical point c^- for $f^5_{\alpha,8}$. The trapping region is a rectangle having one corner on the smallest fixed point of $f^5_{\alpha,8}$ greater than c^- and the other corners as pictured. Note the remarkable quadratic-like nature of the graph of $f^5_{\alpha,8}$ in the trapping region—it clearly resembles that of an upside-down logistic map. As discussed in [1], while L_k is concave down, $L_k(0.5)$ increases with increasing k (so

the concave down hump moves up with increasing k). The difference and the source of the reverse bifurcations in our case is that the graph of $f^5_{\alpha,8}$ is concave up near c^- and $f^5_{\alpha,8}(c^-)$ increases with α (the concave up hump moves up with increasing α). The entire range of orbit behavior exhibited in Fig. 1 appears in Fig. 9, though with orientation reversed.

5. Conclusion

We have provided an example of a family of unimodal maps which exhibits both forward and reverse period-doubling and tangent bifurcations. This family arises from a simple queueing model, and as such the regular and chaotic orbits can be interpreted in terms of changes in a queue length over time.

Our example was found by restricting a bimodal map to an invariant interval on which the function has one hump. One can naturally consider the dynamics of the bimodal map $f_{\alpha,\lambda} : [0, 2] \to [0, 2]$ by choosing (α, λ) in the white region in Fig. 7. As there are two critical points, there now exists the possibility of having *two* distinct stable cycles for one (α, λ) pair. This *bistability* does indeed exist, as seen in Fig. 11.

In general, the addition of the second hump complicates matters significantly in terms of seeking to understand orbit behavior (see [7] and references therein). For our bimodal family the orbit diagrams, which now may differ for $\mathcal{O}^+(c^-)$ and $\mathcal{O}^+(c^+)$, are even yet more complicated (see Fig. 12). The reader might enjoy numerically investigating such diagrams which, at this point, are not completely understood.

References

[1] Frame M, Meachem S. Reverse bifurcations in a quartic family. Computers and Graphics 2000;24:143-149.

[2] Devaney R. An introduction to chaotic dynamical systems, 2nd ed. Boulder, CO: Westview Press, 2003.

[3] Singer D. Stable orbits and bifurcation of maps of the interval. SIAM Journal on Applied Mathematics 1978;2:260-267.

[4] Milnor J, Thurston W. On iterated maps of the interval. In: Alexander J, editor, Dynamical Systems. New York: Springer, 1988. p. 465-563.

[5] Feichtinger G, Hommes C, Herold W. Chaos in a simple deterministic queueing system. ZOR – Mathematical Methods of Operations Research 1994;40:109-119.

[6] Walsh J. The dynamics of circle homeomorphisms: a hands-on introduction. Mathematics Magazine 1999;1:3-13.

[7] LoFaro T. The dynamics of symmetric bimodal maps. International Journal of Bifurcation and Chaos 1997;12:2735-2744.

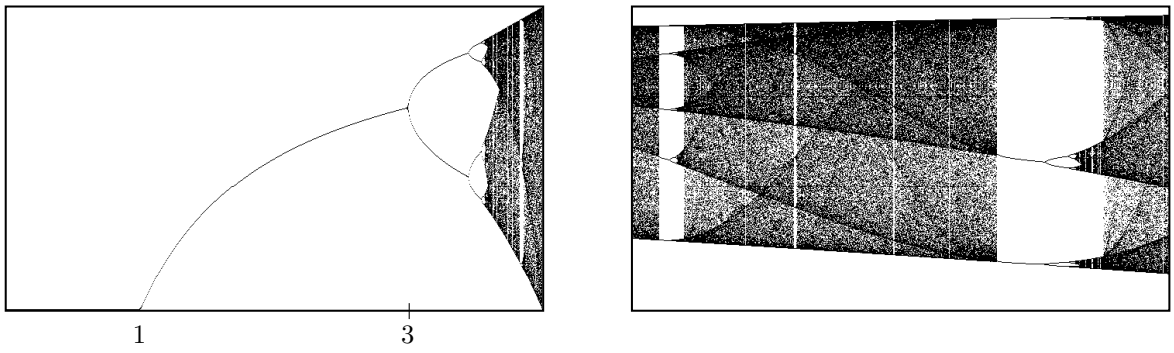

Fig. 1. Left: the orbit diagram for the logistic map. Right: The portion of the orbit diagram for $3.72 \leq k \leq 3.88$. Note the period-5 and period-3 "windows".

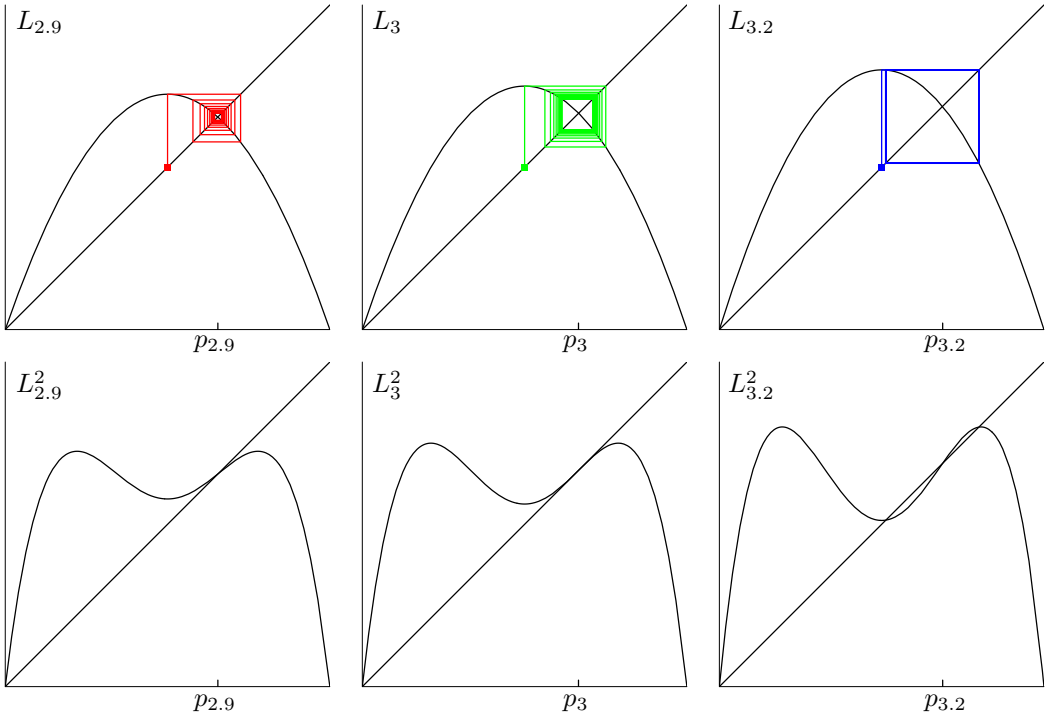

Fig. 2. The period-doubling bifurcation at $k = 3$ is illustrated by graphical iteration. As k increases through 3, the fixed point p_k changes from stable (red) to unstable (blue) and a stable 2-cycle is born. The straight line is the diagonal $y = x$.

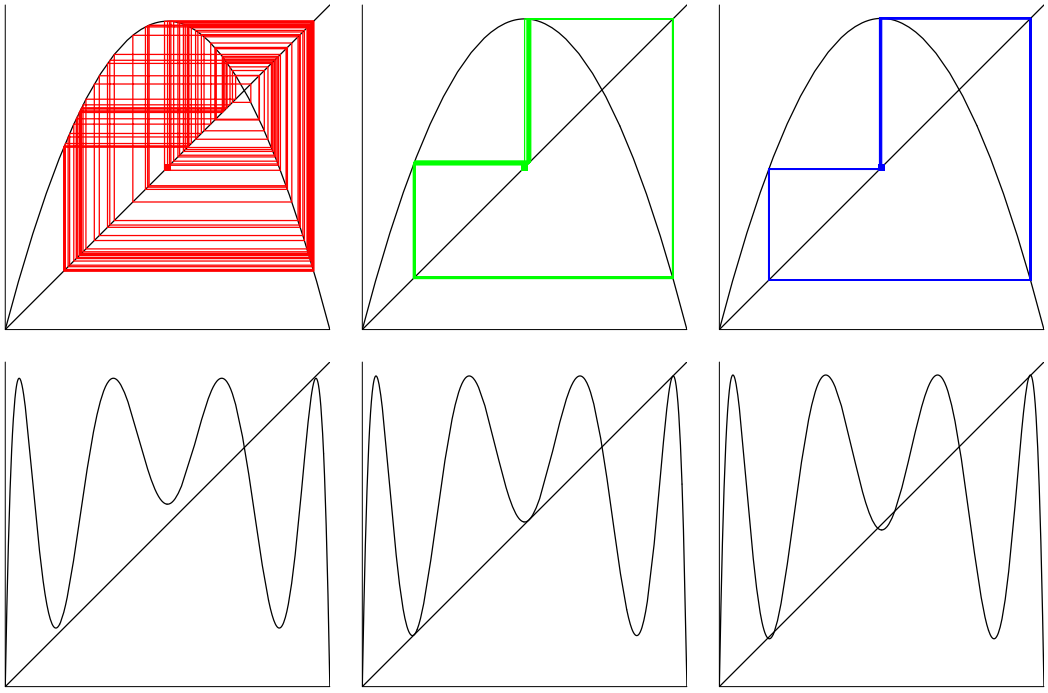

Fig. 3. The tangent bifurcation for L_k^3 is illustrated by graphical iteration. The top row contains graphs of L_k, while the bottom row contains plots of L_k^3. Red: $k = 3.8$. Green: $k = 3.8284$. Blue: $k = 3.84$.

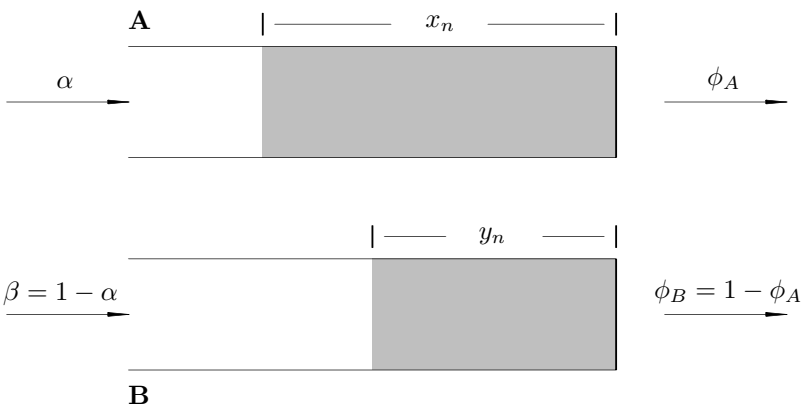

Fig. 4. The model for the queue of size 2.

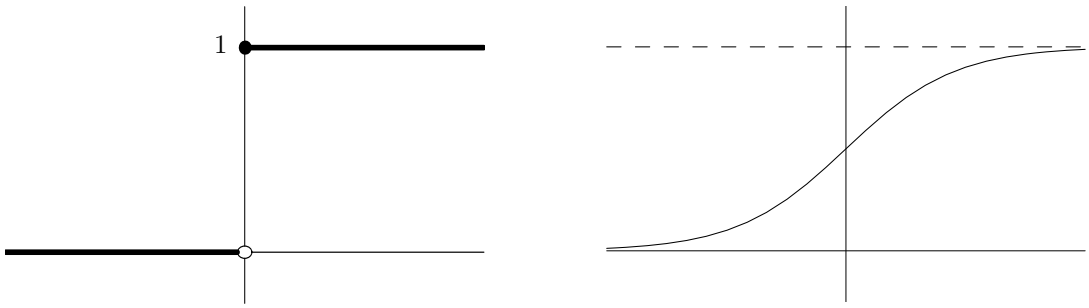

Fig. 5. Two model functions ϕ_A, each a function of the difference in queue lengths $x_n - y_n$. Left: The all-or-nothing model. Right: The S-shaped curve model.

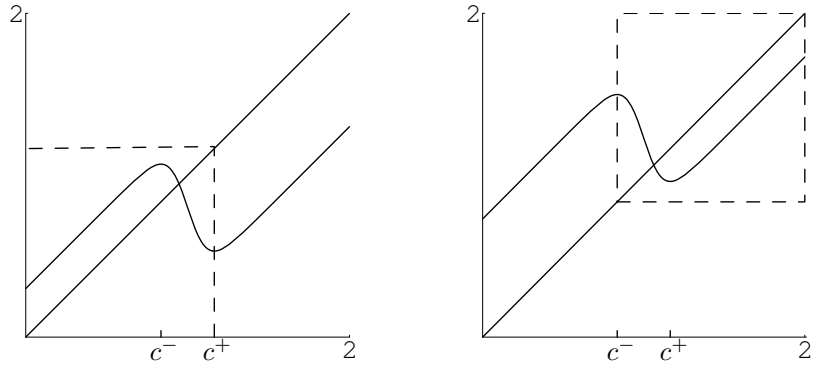

Fig. 6. For $\lambda > 2$, $f_{\alpha,\lambda} : [0, 2] \to [0, 2]$ is a bimodal map. Left: For $\lambda = 8$, $f_{\alpha,8}$ is unimodal on and maps $[0, c^+]$ to itself. Right: $f_{\alpha,8}$ is also unimodal on and maps $[c^-, 2]$ to itself.

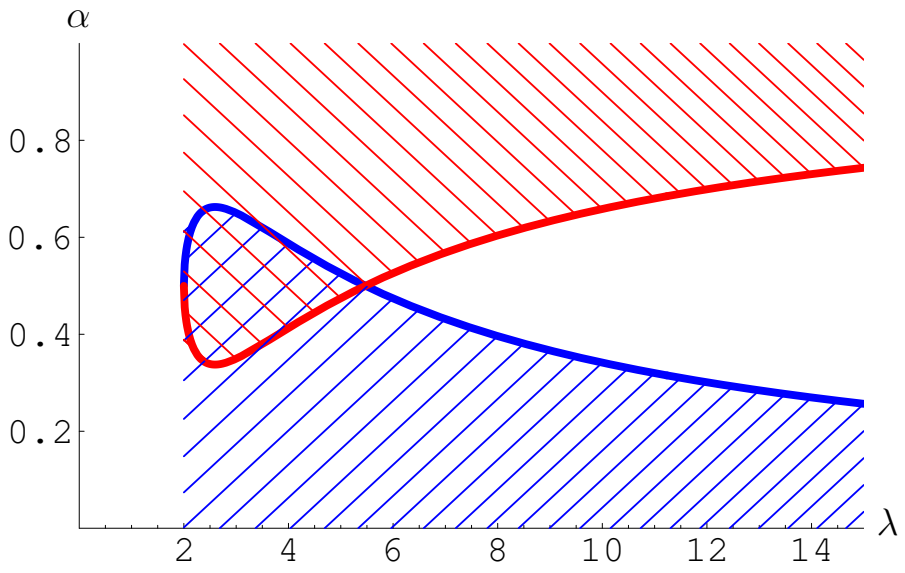

Fig. 7. In the blue region, $f_{\alpha,\lambda}$ restricted to $[0, c^+]$ is unimodal. In the red region, $f_{\alpha,\lambda}$ restricted to $[c^-, 2]$ is unimodal.

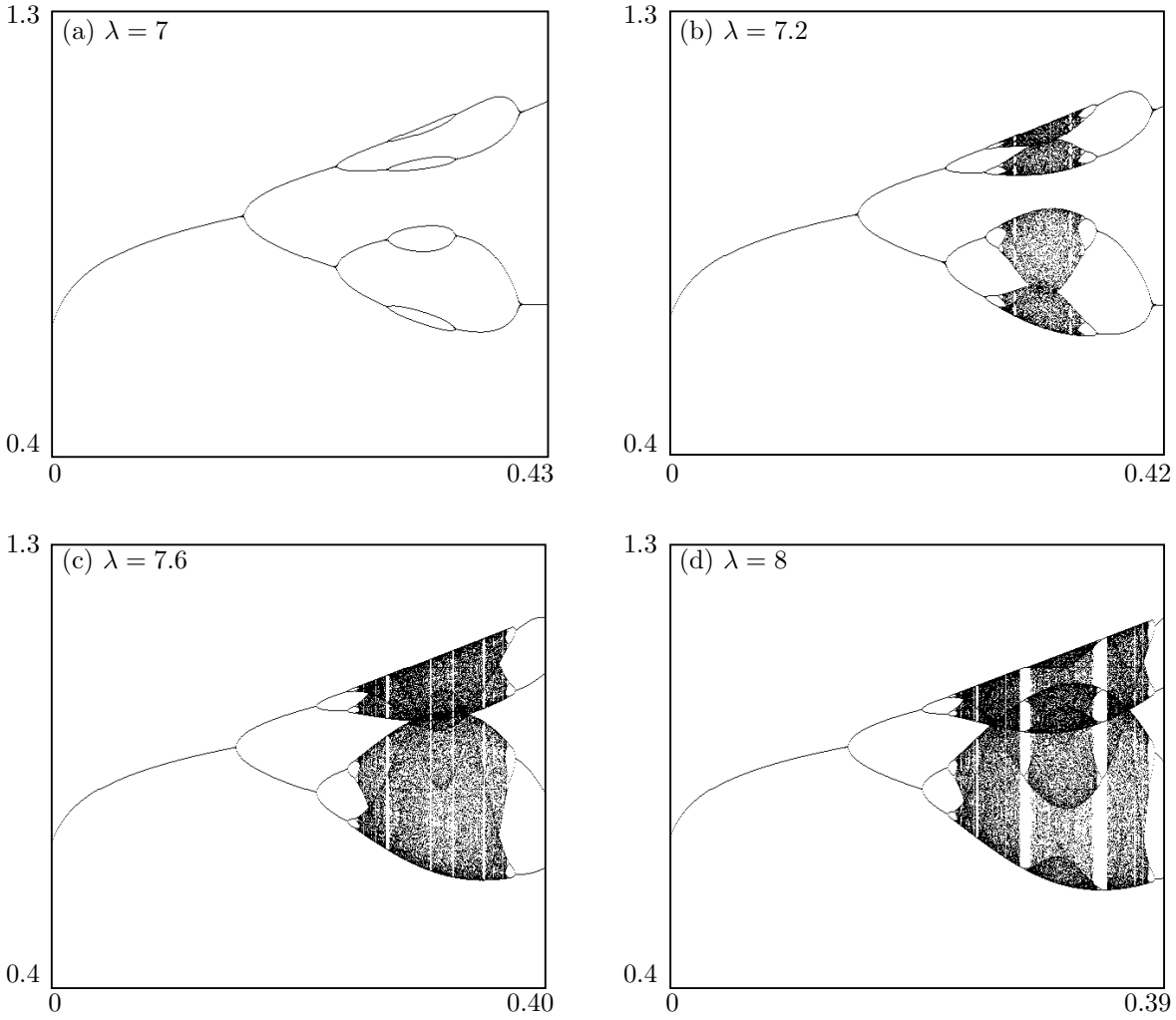

Fig. 8. The long-term behavior of $\mathcal{O}^+(c^-)$ under $f_{\alpha,\lambda} : [0, c^+] \to [0, c^+]$, as a function of α, for $\lambda = 7, 7.2, 7.6, 8$.

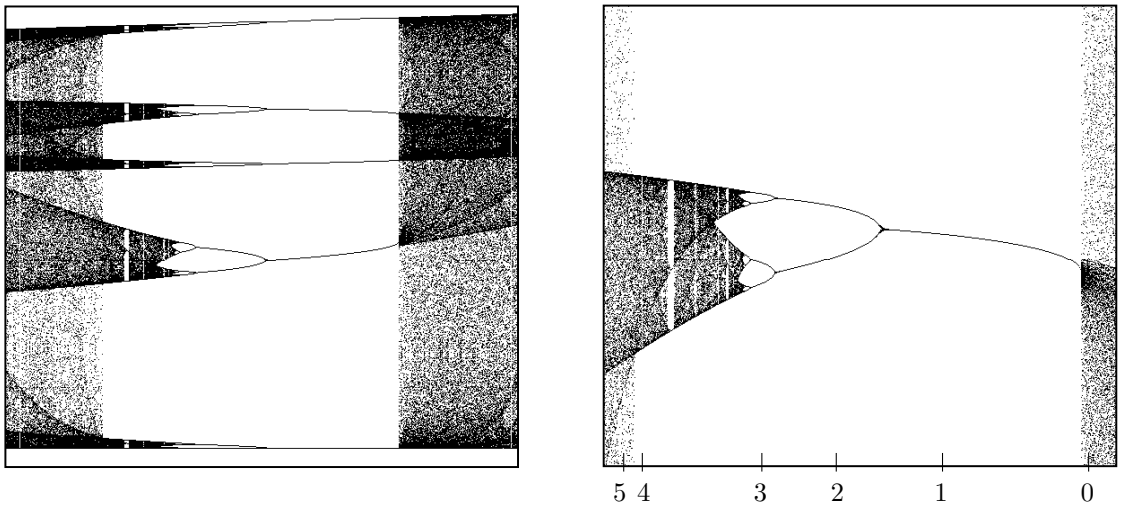

Fig. 9. Left: The period-5 window for $\lambda = 8$ evident towards the right in Fig. 8(d), $0.33 \leq \alpha \leq 0.35$. Right: Zooming in on the branch second from the top in this period-5 window.

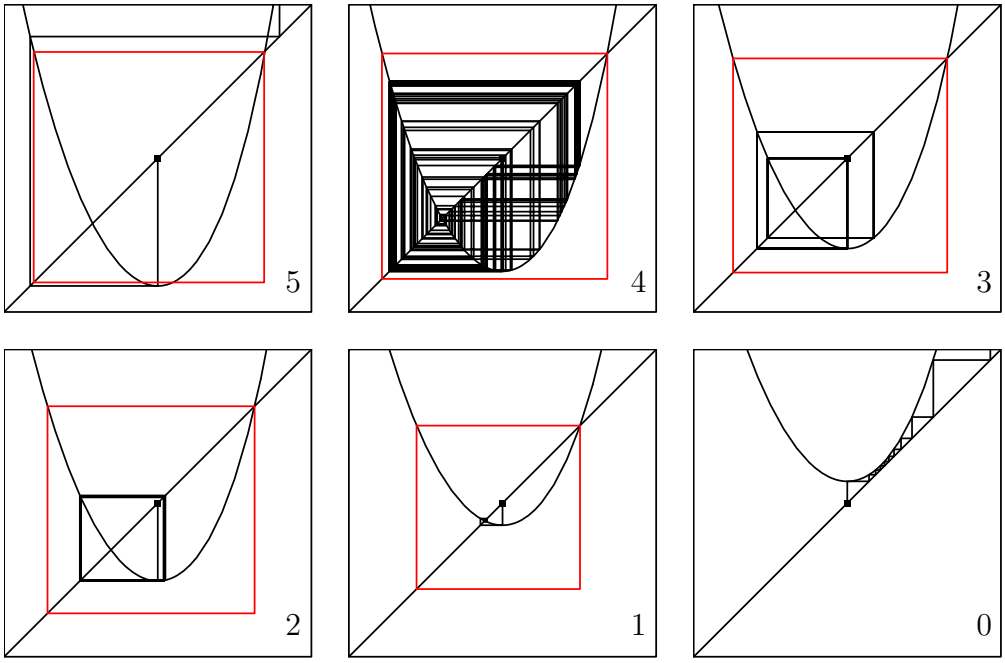

Fig. 10. The graph of $f^5_{\alpha,8}$ in a neighborhood of c^- at the α-values indicated on the right side of Fig. 9. The trapping region, which varies with α, is bounded by the red rectangle.

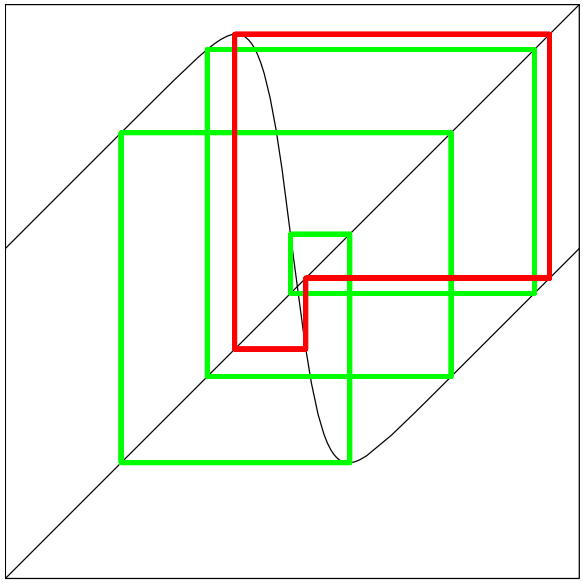

Fig. 11. Bistability for $(\alpha, \lambda) = (0.575, 18)$. The left critical point c^- is attracted to a 3-cycle, while the right critical point c^+ is attracted to a 6-cycle.

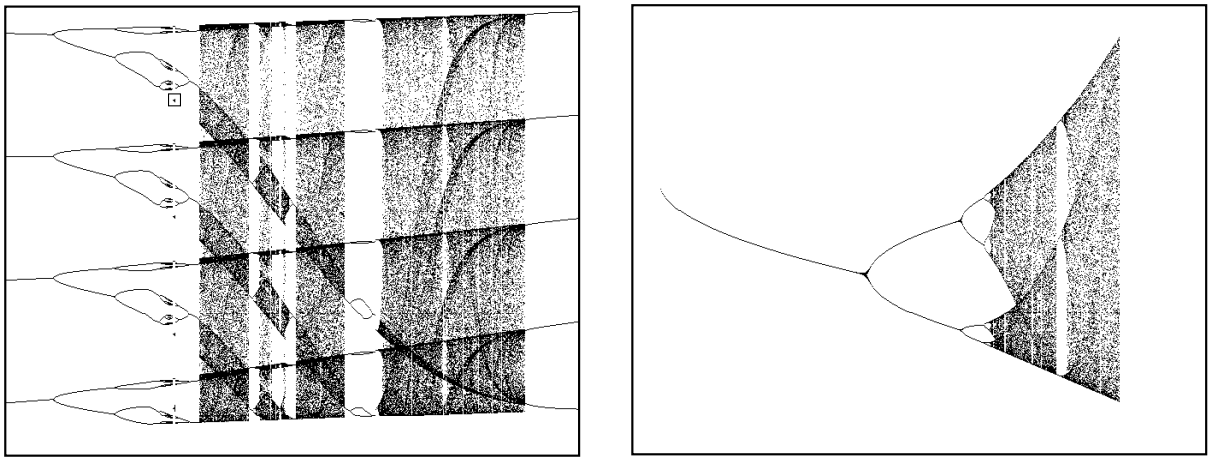

Fig. 12. The long-term behavior of $\mathcal{O}^+(c^-)$ for $\lambda = 21$. Left: $0.76 \leq \alpha \leq 0.8$, $0.82 \leq x \leq 1.7$. Right: Zooming in on the small box in the upper-left quadrant of the bifurcation diagram on the left.